* 전자현미분석기 (EPMA; Electron Micro Probe Analyzer)

EPMA(Electron Probe Micro Analyzer)는 광물학과 암석학, 나아가 고체물리학, 금속학, 무기재료학, 치학에 이르기까지 고체시료 연구에 광범위하게 쓰이고 있는 정량분석이 가능한 전자현미경이다. 다른 전자현미경처럼 이차전자상 (SEI; Secondary Electron Image)이나 후방산란전자상 (BSEI; Back Scattered Electron Image)를 관찰할 수 있으므로, 육안으로는 관찰되지 않는 광물의 미세조직을 관찰할 수 있다. 그러나, EPMA의 가장 중요한 근본적인 기능은 최소 직경 1㎛ 영역의 정확한 화학조성을 알아낼 수 있다는 데에 있다. 이론적으로는 ^{4}Be에서부터 ^{92}U까지 측정이 가능하기 때문에 고체상태시료의 작은 세계를 밝히는데 매우 효과적이다.

▶ 전자현미경은 공통적으로 높은 전압의 전자를 시료에 때려주는 원리를 가지고 있다. 이 때 X선을 비롯한 여러 종류의 전자들이 튀어 올라오고, 이는 시료의 표면상태나 성분과 관련이 있다. 그러므로 원하는 목적에 따라 검출기를 설치하면, 원하는 종류의 전자현미경이 되는 것이다. 흔히 전자현미경이라고 하면 SEM (Scanning Electron Microscope)과 TEM(Transmitted Electron microscope)을 뜻하지만, EPMA도 그 원리상 전자현미경과 다를 바가 없다.

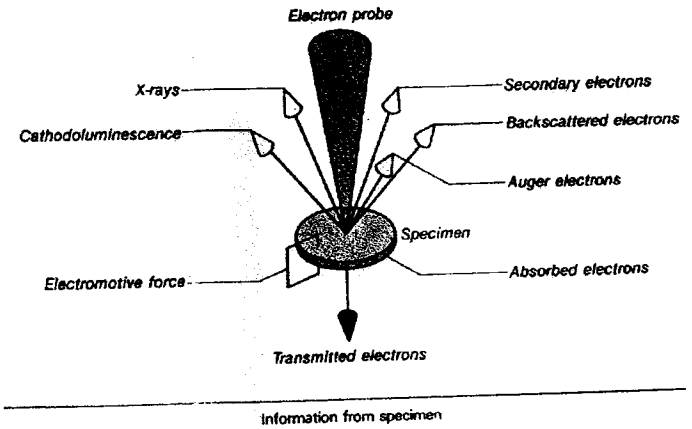

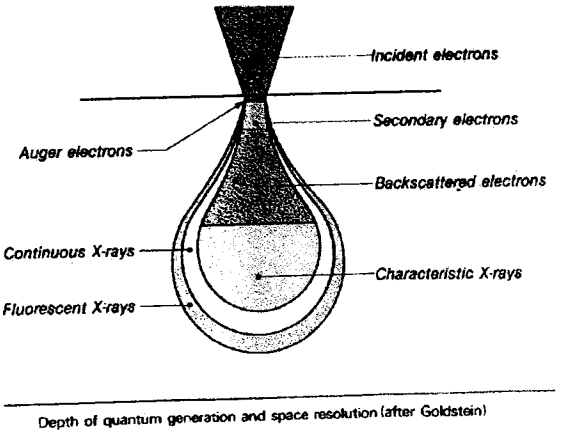

▶ EPMA는 크게 전자를 발생시켜 시료에 투사하는 전자광학장치(Electron Optical System)와 검출기로 나누어져 있다고 할 수 있는데, 검출기에는 이미지를 얻을 수 있는 SEI, BSEI detector와 화학분석을 할 수 있는 WDS (Wavelength

dispersive X-ray Spectrometer)와 EDS (Energy dispersive X-ray Spectrometer) 두 종류가 있다. EDS는 대부분의 SEM에도 쉽게 부착할 수 있으며 상표이름인 EDAX로도 많이 알려져 있는데, 분석이 쉽고 빠르지만 정확성과 분해능이 떨어지며 함량이 적은 원소는 분석하기가 힘들다. 반면, WDS는 분석이 사전작업이 상당히 복잡하지만 매우 정확하며 (유효숫자는 소수점아래 두자리) 최근에는 수십 ppm정도의 원소 측정법도 보고되었다.

▶ EPMA를 비롯한 대부분의 정량분석 장치는 정확한 값을 알고 있는 표준시료를

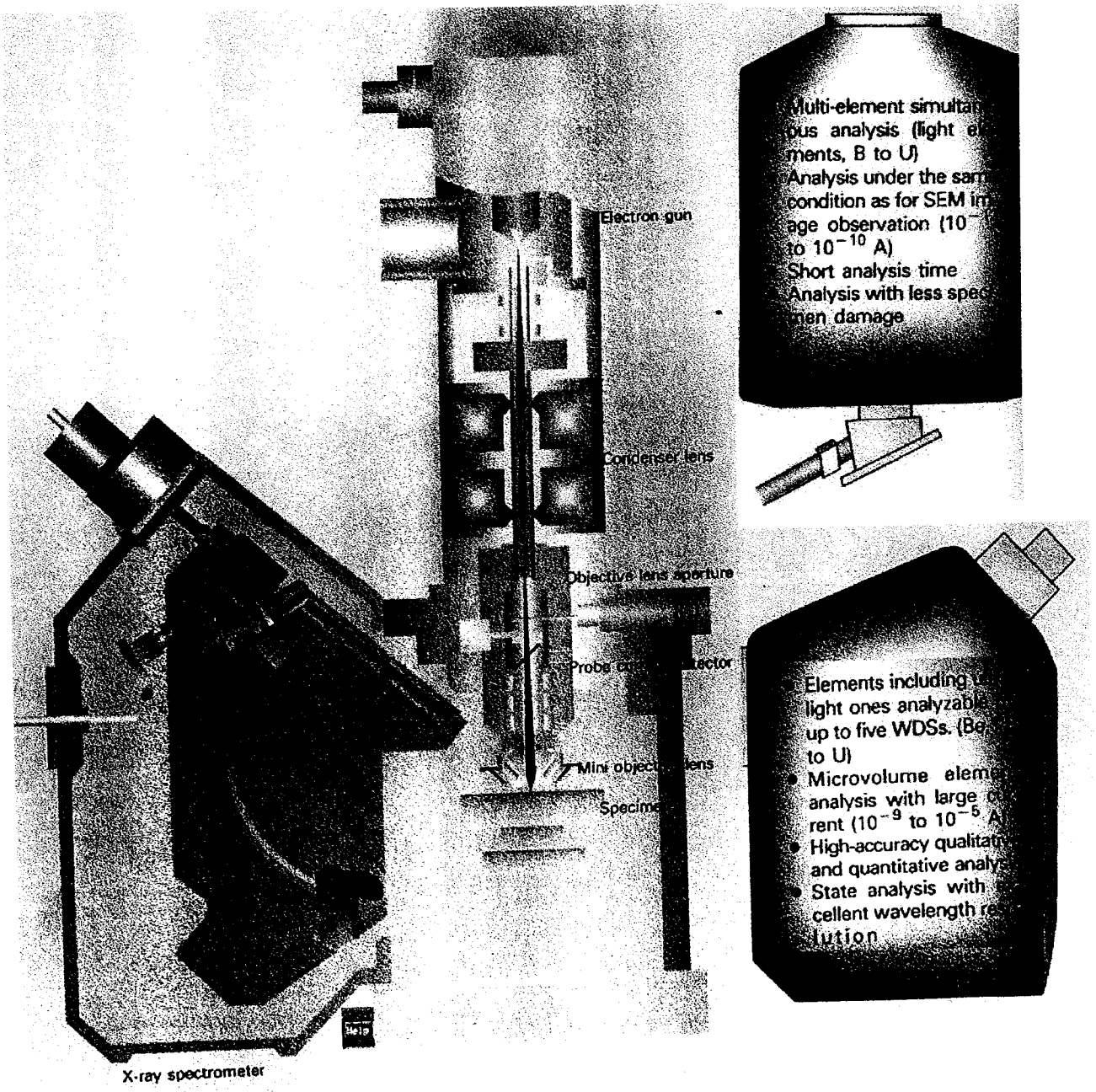

측정한 뒤 그 값과 미지의 시료를 비교하여 정량값을 구하는 방법을 사용한다. 그러므로, 표준시료를 사용한 표준화작업 (Standardization or calibration)이 매우

(사용) whole-rock analysis (전암시료 분석)

X-ray Fluorescence (XRF) 원소함량 분석 (전암분석)

This method uses an X-ray beam of fixed wavelength (such as Cu Kα) to bombard a sample with X-rays and then determine what elements are present based on emitted wavelengths of secondary X-rays (Figure 9.11). The tube works by using a high voltage power supply to accelerate electrons toward a metal target, which then generates X-rays. The type of metal in the target in turn affects the energies of the released X-rays. When X-rays of just the right energy hit your unknown sample, they cause the atoms in the sample to eject inner shell electrons, as noted above. Photons are emitted when outer shell electrons fall down to take the place of the ejected one (fluorescence). The energy of the photon is characteristic of the element present, and depends on the energy difference between the outer shell and the inner-shell electrons (Figure 9.7). Diffraction gratings are used to collect the photons generated by the fluorescence of each element in the sample. The gratings or crystals are set up to diffract only the X-rays of interest to the analysis, and the crystal and detector can be rotated to the correct angle for this diffraction to occur. Analysis of a multielement sample will thus produce a spectrum with distinct peaks for each element and its associated transitions.

강자 ← 특히 lithophile elements (친석원소)

① 미량원소 분석에 강함. (< 1000 ppm)

② Oxide 분석에 강함. (wt. %)

SiO_2
Al_2O_3
K_2O
Na_2O
CaO
MgO
FeO (total Fe) — Fe_2O_3 (Fe^{3+}), FeO (Fe^{2+}) 구분X.
MnO
P_2O_5
TiO_2 ...

X-ray intensities are measured for each element in an unknown (Figure 9.12) sample and compared against intensities of the same elements in a standard. Concentrations are calculated using this relationship, by determining the proportionality constant that relates the concentration of each element to the intensity of its X-rays:

$$\left(C^{\text{element}}_{\text{standard}} = K \, \text{Intensity}^{\text{element}}_{\text{standard}}, \right)_{//}$$

where $C^{\text{element}}_{\text{standard}}$ is the concentration of the element in the standard, $\text{Intensity}^{\text{element}}_{\text{standard}}$ is the intensity of the fluorescence peak at the appropriate energy (see Table 9.2), and K is the proportionality constant. Once a value of K has been determined, then it can be applied to the analysis of unknown minerals where the peak intensity can be meas-

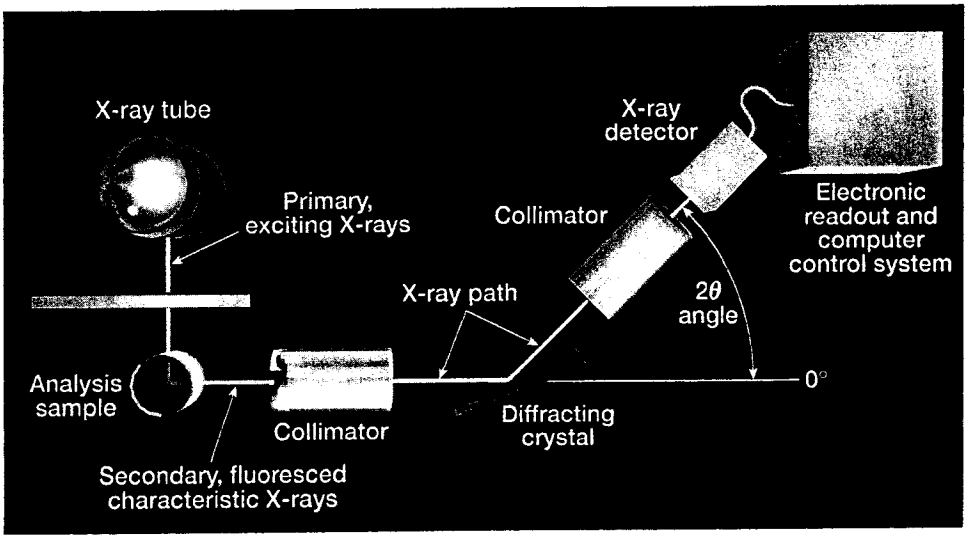

Figure 9.11. A schematic representation of an XRF. An X-ray source shines X-rays onto the sample. In turn, some of these X-rays are diffracted into a detector. This configuration is similar to that of an X-ray diffractometer, which will be explained in more detail in Chapter 15.

XRF ; powder (~200 mesh) → cake → XRF. 바타적 분석.

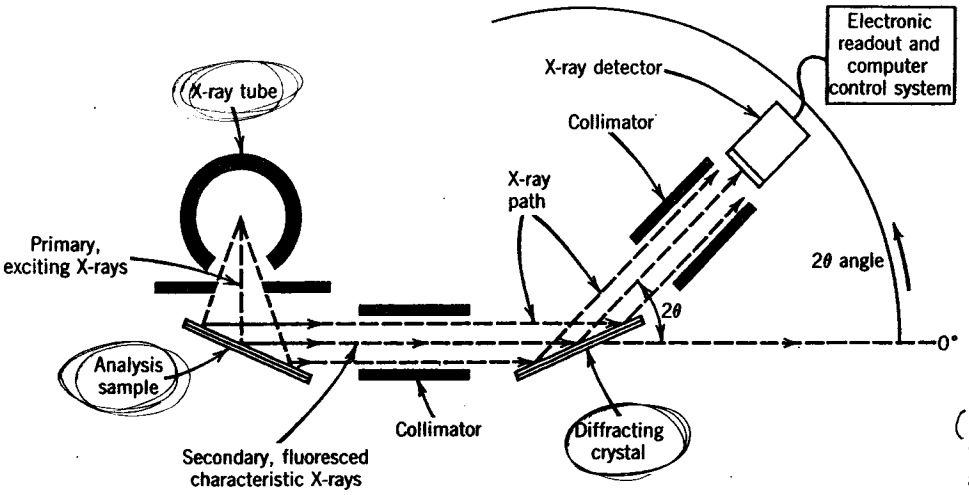

(**FIG. 7.56.**) Schematic illustration of the major components in an X-ray fluorescence analyzer.

Standard sample에서 발생되는 X-ray intensity와
∧ Sample X-ray intensity 비교.
Unknown

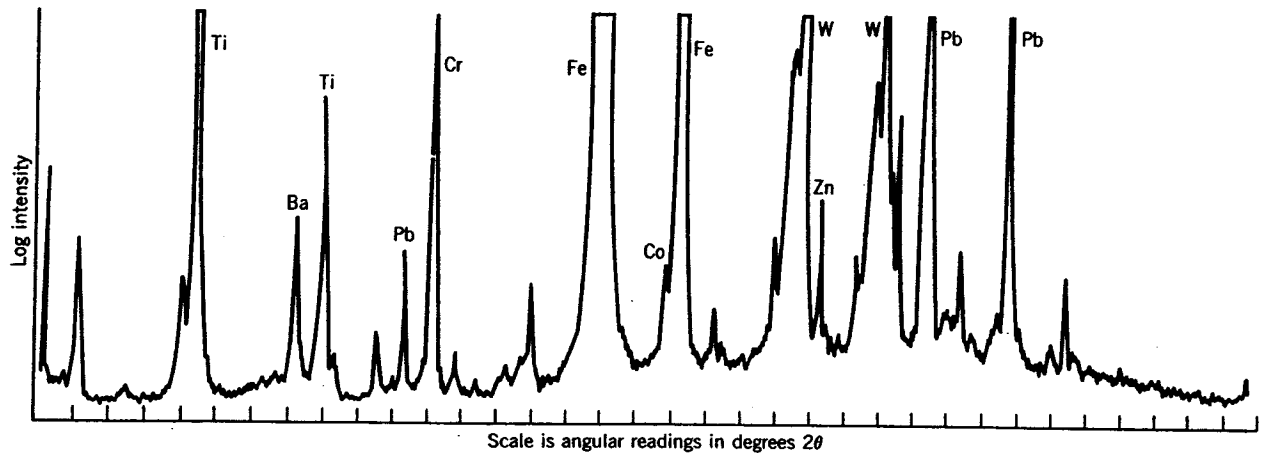

FIG. 7.57. Chart recording of the X-ray fluorescence spectrum obtained of elements present in a genuine bank note. The elements responsible for specific peaks are identified. The W peaks are due to the X-ray tube used with a W target; they are not part of the chemical composition of the bank note. The horizontal scale is in angles of 2θ, expressed as degrees. (From H. A. Liebhafsky, H. G. Pfeiffer, E. H. Winslow, and P. D. Zemany, 1960, *X ray Absorption and Emission in Analytical Chemistry.* New York: Wiley.)

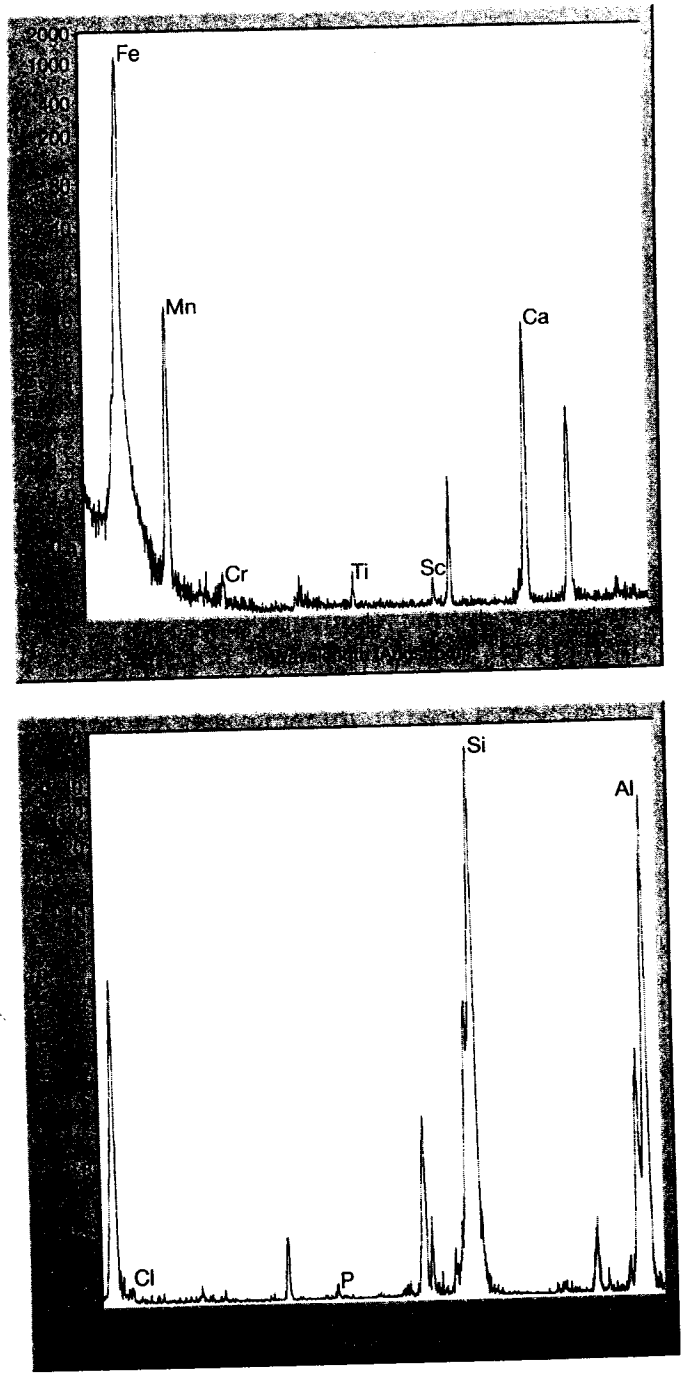

Figure 9.12. XRF spectra of a garnet. Peaks represent electron transitions. Each transition set can be matched to an element. Some of the peaks are identified. Notice that wavelength is plotted along the horizontal axis. Atoms with higher atomic numbers plot at lower wavelengths.

ured, so the concentration can be calculated (c.f. Jenkins, 1999). In practice, this formulation only really works when the concentrations in the standards are roughly the same as those in the unknowns. In other situations, multiple standards and complex calculations to solve for all the interfering effects are required.

Samples are usually prepared for analysis by powdering and then melting them into glass pellets (Figure 9.13), sometimes with the help of a flux to make them melt at a lower temperature (see Buhrke et al., 1997). Once the pellets have been made and a standard has been analyzed, the actual analysis of an unknown takes only a few minutes. A typical XRF unit can measure all the elements in the periodic table that are heavier than oxygen, and detect them at levels as low as parts per million (ppm); light elements are difficult to analyze with this technique. Although the XRF technique was first developed for use on geological samples, advances in technology have also made this a useful tool for many industrial applications, such as quality control! Analyses can also be made on microscopic scales (Janssens et al., 2000).

Electron Microprobe and the Scanning Electron Microscopy

Both electron microprobes (EPMA) and scanning electron microscopes (SEM) combine the capability to image minerals at very small scales with the ability to analyze chemical compositions at those same scales. While the two methods are similar, there are some slight differences. Both instruments can cost $100,000–$700,000 and fill an entire room (Figures 9.14 and 9.15). EPMA requires greater care in sample preparation (the samples must be flat and polished), while angular mineral grains are often analyzed with the SEM. In general, the SEM will yield less accurate and precise chemical data than the EPMA. However, the SEM can be a great aid in identification of minerals, while the EPMA is usually used to characterize minerals. These methods are the most commonly-used tools for determining the chemical composition of minerals. They represent non-destructive techniques capable of rapidly (typically less than 1 minute) analyzing samples on spots as small as a few microns, and sample preparation is very simple.

Electron beam instruments operate somewhat like the XRF with one important difference: they use a beam of electrons, rather than X-rays, to excite the atoms in a specimen. The advantage is that an electron beam can readily be focused to micron spot sizes, whereas this is difficult to do with X-rays. The electrons in the beam are typically accelerated from an electron gun to energies from 15–20 KeV (Figure 9.17). The beam interacts with the mineral sample and excites some of the electrons in the mineral to energy levels above their ground state (which is the lowest energy

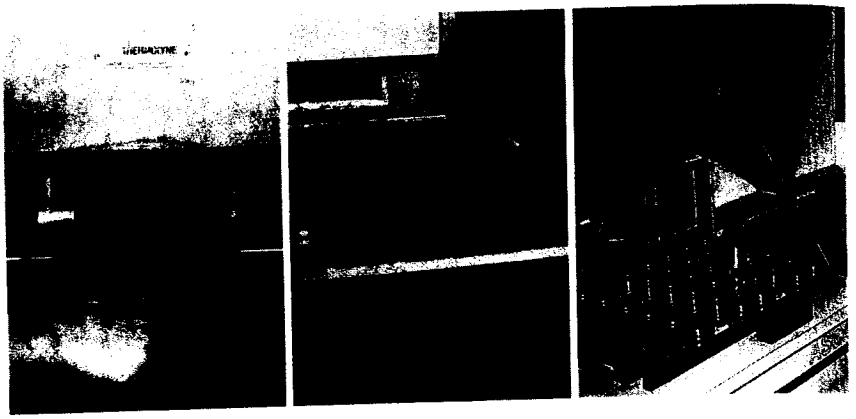

Figure 9.13. *The sample preparation for XRF analysis requires that the mineral be melted into a glass; its surface is then polished. The melting is required to homogenize the sample.*

state). When the excited electrons fall back to their ground states, they fluoresce and emit X-rays (this process should sound familiar from above). Due to the laws of quantum mechanics, the emitted X-rays have very specific wavelengths, or energies, depending upon which elements produced them. The intensity of energy given off at any specific wavelength depends on the concentration of the element in the sample.

Scanning electron microscopes yield high-quality images (Figure 9.16) of minerals as well as semi-quantitative chemistry. The images are created by scanning back and forth over an area of interest and measuring a signal at each pixel. The resultant images look like optical microscopic images, but they're not! The meaning of the image depends on the signal that is recorded by the SEM. **Secondary-electron images** are most sensitive to surface topography and commonly image the morphology of fine-grained minerals. **Backscattered-electron (BSE) images** show contrast in average atomic number and are useful to distinguish elemental distribution of minerals (Figure 9.16). Heavier atoms (e.g., Mn or Fe) tend to backscatter electrons more efficiently and thus, they appear brighter in BSE images than atoms with lower atomic numbers (e.g., Mg or Si), which appear darker. As a result, BSE images convey both morphological and compositional information. SEM's used by mineralogists are normally equipped with **energy-dispersive** (see below) **spectrometers (EDS)** to allow them to analyze X-rays from the sample. An example of an EDS spectrum for a garnet obtained on an SEM is shown in Figure 9.17. Notice how the peaks are plotted as a function of energy. Compare this to the XRF output (Figure 9.11) for a garnet, where the peaks are plotted as a function of wavelength. The combination of morphological information obtained from imaging and compositional data gained from BSE and EDS is extremely powerful in mineral identification.

Electron microprobes (EPMA) for electron probe microanalysis are very similar to SEM's and can also create nice images of minerals particularly elemental maps (Figure 9.19). However, they are optimized for analyzing the X-rays that are emitted from minerals (and other materials, of course). The electron gun on an EPMA system can be up to 1000 times brighter than on an SEM, resulting in an electron beam that generates a lot of fluorescence! The wavelength and intensity of the emitted X-rays are analyzed with one of the two types of detectors. **Energy dispersive spectrometers** (EDS) can simultaneously count the number of X-ray photons emitted from a mineral and analyze the energy of each photon, thereby identifying the element that emitted that photon. In contrast, **wavelength-dispersive spectrometers** (WDS) have crystals that are individually tuned to the wavelength of the X-rays emitted by an element of interest (Figure 9.18). Elements from beryllium (Z = 4) to uranium (Z = 92) can be analyzed under optimal conditions. Although this may seem like a more cumbersome method,

In everyday usage, the terms "precision" and "accuracy" are often taken to mean the same thing. However, to an analyst, these terms have very specific, distinct meanings.

Precision effectively means the same thing as reproducibility. It is a measure of how well you can perform an analysis in repeated operations. You can think of it as the degree of perfection in your analysis.

Accuracy describes the difference between the true (or accepted) answer, and the one that you have measured.

To summarize, precision reflects how well you can do the analysis, and accuracy reflects the relationship between your answer and the "truth." A good analyst strives for both high precision and high accuracy.

EXERCISE 22

Identification of an Unknown by X-Ray Powder Diffractometer Tracing

PURPOSE OF EXERCISE

To understand the steps involved in the identification of an unknown mineral using the diffractometer tracing of its powder diffraction effects. As in exercise 21, you will need to refer to the Powder Diffraction File of the International Center for Diffraction Data.

FURTHER READING

See listing in exercise 21, p. 295.

Background Information: If you have completed exercise 21 before beginning this assignment, you will find that identification of unknown crystalline materials is a great deal faster by diffractometer technique than it is by film. This is because a diffractometer tracing provides you with a graphical display of each peak position, relative to a direct reading 2θ scale, as well as a reasonably quantitative, direct reading, relative intensity scale.

A powder X-ray diffractometer is a great deal more complex and expensive than a powder camera mounted on an X-ray generator. A diffractometer, in conjunction with an X-ray generator, consists of a goniometer (a device that measures the angular location in terms of 2θ for a diffraction peak), an X-ray counting device (such as a Geiger, a scintillation, or a proportional counter for measurement of peak intensity), and an electronic readout system (see Fig. 22.1). On nonautomated powder diffractometers the graphical result is a diffractometer chart obtained over a 2θ region of about 6° to 80°, during a time period of about 45 minutes. On an automated diffractometer the same results are printed out on an $8\frac{1}{2} \times 11$-inch page in about 15 minutes. In either case, the final diagram shows peak locations with respect to a horizontal 2θ scale, as well as relative intensities of the peaks in terms of a vertical scale. To search the diffraction files for identification of an unknown, an investigator needs at the minimum to convert the 2θ values of the three most intense peaks on the graph to *d* values [using the *X-ray Diffraction Tables* of Fang and Bloss (1966), or, if these are not available, by using Table 21.1, or by solving the Bragg equation as outlined in section 2 of assignment 21]. It is strongly suggested, however, that to be certain the identification is completely unambiguous, the investigator should compare the *d*s of another ten or so peaks in the pattern with the published pattern on which the identification is based. Even though the identification of an unknown is based on matching of the three most intense X-ray diffraction lines, all other lines in the unknown pattern and those of the selected matching reference pattern should show good agreement in *d* values and intensity.

MATERIALS

The diffractometer tracing in Fig. 22.2 and Table 22.1 for data tabulation. A 90° triangle is useful for locating peak positions accurately on the diffractometer tracing with respect to the horizontal 2θ scale. You need access to the 2θ-to-*d* conversion tables of Fang and Bloss (1966), *X-ray Diffraction Tables*. If these are not available, the 2θ values can be converted to their appropriate *d*s by solving the Bragg equation with the help of an electronic calculator. Figures 22.3 and 22.4 should allow for unambiguous identification of the unknown. To check the *d*s and the intensities of all the diffraction lines on the pattern, you will need access to a microfiche or card edition of the file of the International Center for Diffraction Data.

ASSIGNMENT

1. Using the diffractometer tracing in Fig. 22.2, assign 2θ values to each of the peaks. Carefully locate each peak position with reference to the horizontal 2θ scale. Write the 2θ appropriate to the peak next to it on the figure. Number the peaks from left to right. Enter the peak numbers and 2θ values into Table 22.1.

2. Read the relative intensities of all the peaks, by measuring the height of the peak on the vertical scale and subtracting the background value in the area of the peak. Assign the value of 100 to the most intense peak. If the height of the tallest peak is *y* divisions (where *y* is some number less that 100), multiply all the other peaks by the ratio of 100/*y* to obtain their values relative to 100. Enter these relative peak heights into Table 22.1.

3. Convert the 2θ angles to *d* values using the *X-ray Diffraction Tables* of Fang and Bloss, or Table 21.1, or calculate each *d*, using the Bragg equation as outlined in section 2 of the assignment in exercise 21. Because the pattern shows no $\alpha_1 - \alpha_2$ doublets, use the CuKa column in Fang and Bloss.

4. Using the *d* values of the three most intense peaks, identify the substance with Figs. 22.3 or 22.4.

FIGURE 22.1 Schematic diagram of some of the experimental configuration of an X-ray powder diffractometer.

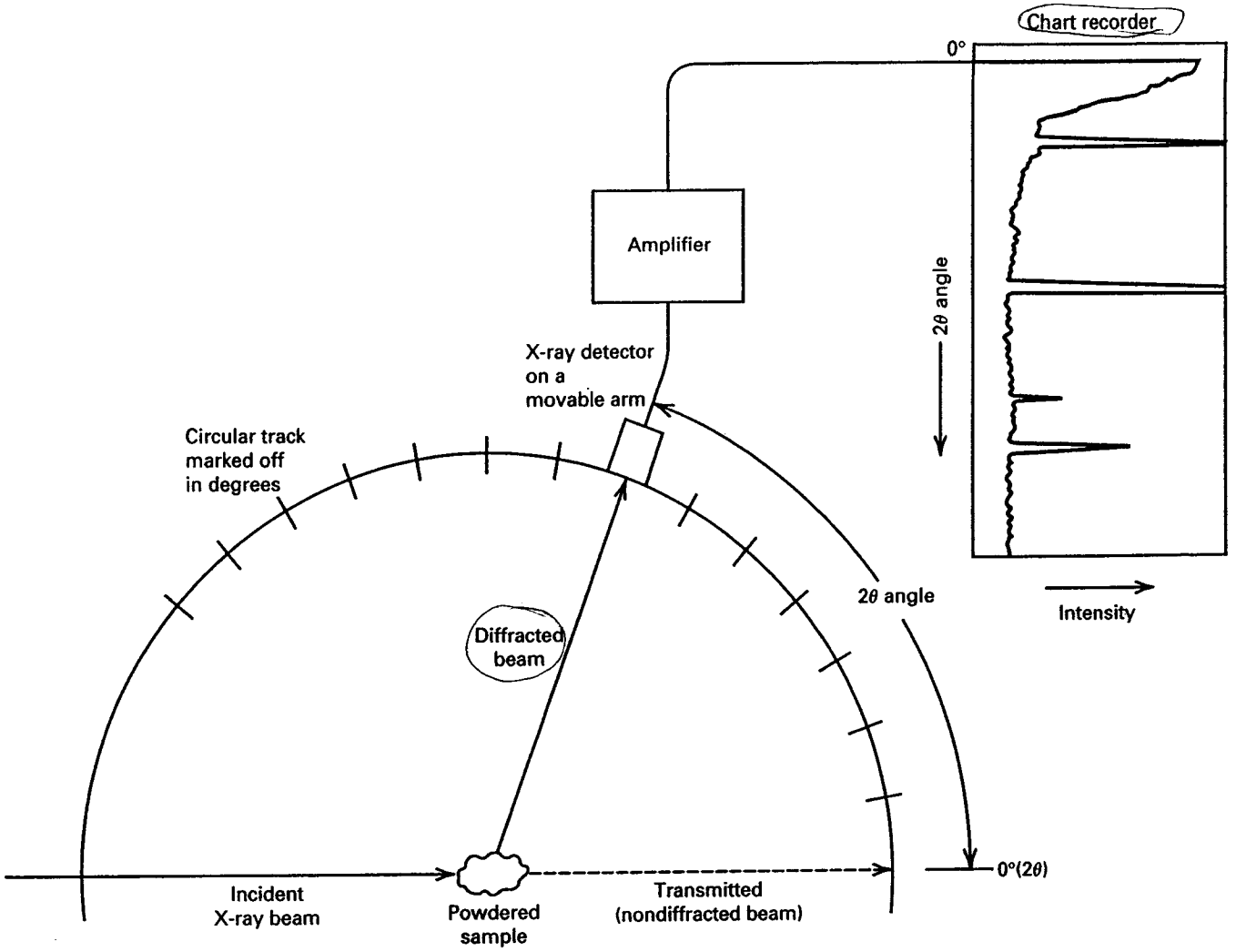

5. After identification, make sure the additional five *d* values listed in Figs. 22.3 or 22.4 show good agreement with the data from your pattern.

6. If search files from the International Center for Diffraction Data are available, locate the complete reference card on the substance and make sure *all* peaks and their intensities of both the "unknown" and the substance you identified it to be show good correspondence.

EXERCISE 22

Student Name

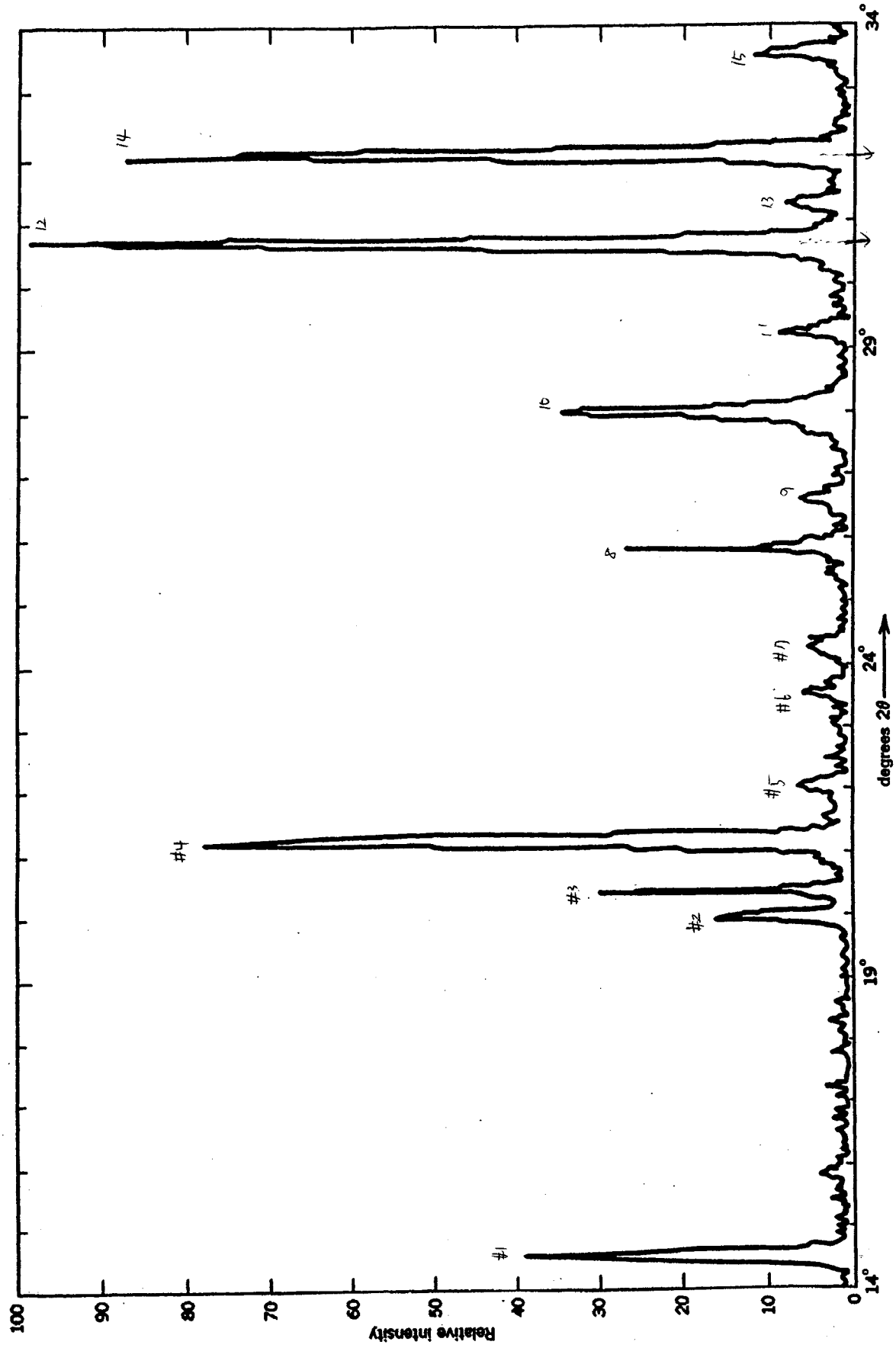

FIGURE 22.2 Diffractometer tracing for the unknown that is to be identified in this exercise. The X-ray radiation was produced by a Cu target X-ray tube. The 2θ-angle scale is horizontal. The relative intensity scale is vertical.

EXERCISE 22

Student Name

TABLE 22.1 Record of Measurements Obtained from the Diffractogram in Fig. 22.2. Refer to the diffractogram in Fig. 22.2.

Line Number[a]	*2θ angle*	*d*	*I*
1	14.5		
2	20.0		
3	20.5		
4	21.0		75
5	22.0		
6	23.5		
7	24.5		
8	26		
9	26.5		
10	28.0		
11	29.0		
12	30.5		100
13	31.5		
14	32		90
15	33.5		

Published 2θ values for the three most intense lines in the pattern of Fig. 22.2.

2θ	I
30.62	100
31.97	90
21.06	75

$d = \frac{\lambda}{2\sin\theta} = \frac{1.5418}{2\sin 30^\circ} = \frac{1.5418}{2 \times \frac{1}{2}} = 1.5418$

[a]Line numbers go consecutively from left to right.

Mineral identified as: _____

Diffraction file no.: _____

$\lambda_{Cu} = 1.5418\ \text{Å}$

$d = \frac{\lambda}{2\sin\theta}$ 2 THAT

FIGURE 22.3 A page from the *Search Manual* (Hanawalt Section) of the *Powder Diffraction File*, for Inorganic Phases, 1986. The *d* values for families of planes that produce the eight strongest diffraction lines from a specific substance are listed. The number of the complete reference file card is given in the right column. (Reproduced by permission of the International Center for Diffraction Data.)

d value ⟶

									2.94 – 2.90 (±.01)	File No.	I/Ic
	2.90,	2.82,	2.00,	3.98,	3.47,	2.68,	1.88,	2.03,	$Ca_2(AsO_4)_2(OH)$ Johnbaumite	23- 265	
i	2.90,	2.82,	2.30,	2.23,	1.69,	4.47,	3.81,	3.16,	Ti_3I_2	24-1310	
	2.90,	2.82,	2.33,	1.21,	1.69,	1.34,	1.32,	2.78,	GeSm	20- 436	
	2.90,	2.82,	2.31,	2.68,	3.11,	3.00,	2.61,	2.36,	$K_2H_2(CO_3)_2 \cdot 1.5H_2O$	20- 864	
	2.89,	2.82,	2.06,	2.06,	2.29,	2.98,	2.55,	2.71,	$Ca_3Si_2O_{12} \cdot H_2O$	14- 35	
	2.89,	2.82,	2.84,	2.01,	1.66,	1.72,	2.47,	1.78,	CaY_2O_4	19- 265	
	2.89,	2.82,	2.78,	2.14,	2.05,	1.99,	1.84,	1.83,	$(Ca,Sr)_2B_5O_9(OH)_2Cl$/Hilgardite-1Tc, strontian	11- 405	
	2.89,	2.82,	2.75,	2.80,	4.69,	4.53,	2.07,	1.96,	La_2CuO_4	18- 673	
	2.89,	2.82,	2.02,	1.66,	2.55,	5.16,	5.02,	1.47,	K_2As	.4- 676	
•	2.93,	2.81,	4.23,	2.69,	8.47,	2.54,	1.71,	1.93,	$LaFeMgO_4$	34- 965	
	2.93,	2.81,	3.39,	2.90,	2.17,	1.99,	1.62,	3.06,	$K_2CaSi_2O_6$	27-1346	
c	2.93,	2.81,	2.79,	1.92,	3.06,	2.16,	2.16,	3.17,	Bi_2Rh	28- 172	
•	2.93,	2.81,	2.14,	1.99,	2.19,	2.59,	1.47,	6.57,	K_2MgF_4	23- 469	
•	2.94,	2.81,	2.55,	2.75,	2.45,	2.34,	2.26,	1.96,	Ba_2MgCl_6	15- 292	
c	2.94,	2.81,	1.88,	5.63,	1.72,	1.47,	3.45,	1.27,	Bi_2Cs	27- 323	
	2.93,	2.81,	8.43,	2.33,	6.16,	4.22,	2.10,	3.32,	$K_4Fe(CN)_6 \cdot 3H_2O$/Kalidihydrocyanite, syn	14- 695	1.80
•	2.93,	2.81,	4.05,	2.03,	2.31,	1.64,	1.84,	2.43,	$Ba_2MgSi_2O_7$	10- 74	
	2.93,	2.81,	3.05,	1.72,	3.11,	2.85,	1.87,	2.50,	$Pb_2Sr_2SiO_6$	30- 728	
•	2.92,	2.81,	4.16,	2.43,	2.63,	3.03,	3.80,	2.49,	Li_2CO_3	22-1141	0.90
•	2.91,	2.81,	4.05,	3.30,	2.44,	4.46,	3.39,	2.57,	$Na_2CO_3 \cdot 7H_2O$	25- 816	
•	2.91,	2.81,	4.04,	2.02,	2.31,	1.83,	1.64,	2.42,	$NaBaPO_4$	33-1210	
i	2.91,	2.81,	3.33,	3.18,	4.21,	1.93,	1.82,	2.02,	$Ba_5(PO_4)_3F$	34- 627	
i	2.91,	2.81,	3.03,	1.80,	2.63,	2.55,	1.77,	1.75,	$Ge_{10}P_{12}$	34- 699	
	2.91,	2.81,	2.96,	2.25,	3.97,	3.48,	2.56,	2.46,	$IrB(OH)_8$	30- 918	
	2.91,	2.81,	2.62,	2.43,	1.70,	1.63,	1.31,	1.30,	$AuPb_3$	24- 711	
	2.90,	2.81,	3.39,	2.95,	2.17,	1.99,	1.62,	3.06,	$K_2CaSi_2O_6$	27-1346	
	2.90,	2.81,	3.18,	3.31,	2.16,	4.20,	2.01,	4.04,	$Ba_5(PO_4)_3OH$	22- 613	
	2.90,	2.81,	2.65,	1.59,	1.47,	1.09,	0.83,	1.73,	Am	15- 657	
i	2.90,	2.81,	2.02,	3.43,	1.66,	2.45,	2.20,	1.64,	$Ba_2Sc_2O_5$	31- 161	
	2.89,	2.81,	4.46,	3.36,	2.09,	1.92,	4.21,	3.14,	$CoAl(SeO_3)_2 \cdot 12H_2O$	26- 278	
	2.89,	2.81,	3.22,	6.79,	2.99,	2.41,	2.01,	1.79,	$(Na,Ca,Mn)_3Zr(SiO_3)_6F$/Lavenite	14- 886	
c	2.94,	2.80,	2.51,	2.20,	2.65,	1.47,	2.72,	2.48,	$Ba_2Zn_2Fe_{12}O_{22}$	25-1193	
	2.93,	2.80,	2.64,	2.91,	2.95,	5.86,	2.86,	2.43,	$PbFe_8O_{13}$	33- 757	
i	2.91,	2.80,	1.98,	1.63,	3.78,	1.70,	2.14,	1.45,	K_2NbO_3	27- 423	
	2.90,	2.80,	4.23,	2.82,	5.60,	2.26,	2.02,	1.79,	Al_4Ba	10- 290	
	2.90,	2.80,	2.95,	2.03,	1.67,	1.66,	2.01,	1.70,	$SrYb_2O_4$	30-1222	
•	2.90,	2.80,	1.90,	3.61,	3.19,	2.03,	1.81,	1.85,	$Ca_2Na_2Sr_3(PO_4)_2(SiO_4)_2F_2$	30- 268	
	2.89,	2.80,	3.21,	2.60,	4.41,	3.58,	3.51,	3.26,	K_2S_5	30- 992	
i	2.95,	2.79,	2.66,	4.12,	2.69,	3.47,	3.39,	3.11,	$Ba_{1.2}Sb_{0.8}O_{1.6}S_{0.4}$	31- 119	
•	2.95,	2.79,	2.03,	1.74,	1.64,	4.37,	3.73,	3.12,	$BaLa_2N_2O_5$	35- 164	
c	2.94,	2.79,	2.96,	2.16,	2.16,	1.53,	1.91,	1.61,	CeO_2	31- 266	3.00
c	2.93,	2.79,	4.66,	5.05,	2.91,	3.23,	3.97,	3.78,	Ba_2F_{10}	33- 172	1.88
•	2.92,	2.79,	4.21,	6.12,	4.36,	3.44,	3.19,	2.45,	α-$LiAlSi_2O_6$/Spodumene	33- 786	
	2.92,	2.79,	2.57,	2.30,	3.60,	3.16,	2.83,	2.62,	$Ca_3SiO_3Cl_2$	34- 558	
•	2.92,	2.79,	2.02,	2.06,	1.48,	1.44,	1.21,	1.46,	Sn/Tm, syn	4- 673	
	2.91,	2.79,	2.94,	2.81,	3.16,	2.58,	0.00,	0.00,	$Sr_2Ge_2O_7$	21-1181	
	2.91,	2.79,	2.74,	3.74,	3.96,	3.93,	2.09,	2.01,	$Pb_2O_2Cl_2$	6- 475	
	2.91,	2.79,	1.96,	1.57,	1.48,	1.27,	2.58,	1.65,	Sr_2N_2	17- 797	
i	2.90,	2.79,	2.78,	1.45,	2.94,	2.02,	2.00,	1.66,	$Sr_2Lu_2O_5$	32-1342	1.90
i	2.90,	2.79,	1.91,	2.01,	3.17,	3.30,	3.60,	1.95,	$Ca_5Sr_4(PO_4)_6(OH)_2$	34- 477	
	2.89,	2.79,	10.8,	4.10,	2.67,	2.48,	2.36,	1.67,	α_2-$Ca_4Al_2O_7 \cdot 19H_2O$	14- 628	
i	2.89,	2.79,	2.59,	2.68,	2.67,	2.40,	2.29,	2.10,	$Ca_2(Al,Fe)Al(SiO_4)_2OH$/Clinozoisite	21- 128	
	2.89,	2.79,	2.15,	2.75,	1.63,	1.61,	1.70,	2.84,	$Sr_3Al_2O_6$	16- 65	
i	2.89,	2.79,	1.98,	1.63,	6.34,	1.68,	2.11,	1.44,	$Sr_2Fe_{1.5}Sn_{0.5}O_5$	32-1238	
i	2.89,	2.79,	1.91,	3.38,	3.16,	2.00,	3.29,	1.95,	$Ca_5Sr_4(PO_4)_6(OH)_2$	34- 478	
	2.93,	2.78,	2.69,	3.11,	4.44,	3.30,	2.42,	5.57,	$Ba_2NaCa_2Fe(Ti,Nb)_2Si_4O_{20}(OH,F)\cdot H_2O$/Joaquinit	36- 385	
i	2.93,	2.78,	3.84,	2.81,	5.00,	4.79,	2.80,	8.51,	$Na_2SiO_3 \cdot 9H_2O$	19-1239	
i	2.93,	2.78,	2.92,	2.89,	3.33,	3.76,	2.15,	1.91,	$Pb_2Mn_2Ge_2O_7$	34-1362	
	2.92,	2.78,	2.57,	2.13,	2.60,	5.71,	4.21,	2.27,	$PbSn_4$	4- 744	
c	2.92,	2.78,	2.41,	2.55,	3.56,	3.20,	3.17,	2.15,	CaCl	25-1138	
•	2.92,	2.78,	2.82,	2.94,	3.26,	3.12,	4.81,	2.37,	$KSrPO_4$	33-1045	
c	2.89,	2.78,	2.99,	2.44,	2.14,	4.78,	3.67,	3.10,	Sb_2Sr	30- 98	6.03
	2.89,	2.78,	2.95,	3.11,	4.44,	3.30,	2.42,	5.57,	$Ba_2NaCa_2Fe(Ti,Nb)_2Si_4O_{20}(OH,F)\cdot H_2O$/Joaquinit	36- 385	
i	2.89,	2.78,	2.66,	2.17,	2.32,	1.87,	2.54,	1.67,	$Na_2AlH_2(CO_3)_2F_2$/Sorensenite	25- 692	
	2.89,	2.78,	2.19,	3.16,	2.68,	2.82,	3.46,	3.26,	$KCa_4F_9O_4$	27-1343	
	2.95,	2.77,	4.72,	2.53,	2.46,	2.36,	2.27,	2.24,	K_2MoO_4	24- 875	
	2.95,	2.77,	3.51,	2.48,	1.20,	1.17,	1.76,	1.72,	La_2Si_2	19- 660	
	2.94,	2.77,	4.01,	2.17,	1.63,	3.44,	2.61,	2.40,	$Ba(BrO_3)_2$	20- 120	
	2.93,	2.77,	3.69,	2.69,	4.68,	2.55,	2.52,	3.51,	$H_4Ag_3NO_4P$	16- 511	
	2.92,	2.77,	3.75,	3.43,	3.08,	2.33,	1.78,	1.54,	$Ag_2V_4O_{11}$	20-1385	
•	2.92,	2.77,	2.01,	1.62,	2.20,	1.60,	1.38,	1.29,	$CeLa_2B_2O_{12}$	36-1278	
	2.92,	2.77,	2.01,	1.46,	1.66,	1.43,	2.06,	0.00,	InSb	19- 579	
c	2.90,	2.77,	5.55,	1.85,	1.70,	2.40,	1.45,	1.25,	Bi_2Rb	28- 175	
i	2.90,	2.77,	3.22,	4.33,	5.87,	3.00,	2.67,	2.51,	$K_2Ba(Ge_4O_9)_2$	31- 975	
	2.94,	2.76,	4.26,	2.09,	1.82,	3.38,	1.29,	5.80,	$DyPO_4 \cdot 1.5H_2O$	21- 316	
•	2.94,	2.76,	2.62,	2.33,	3.23,	3.18,	3.03,	2.90,	Rb_2BiI_5	20- 906	
	2.93,	2.76,	3.05,	2.40,	2.30,	2.16,	2.85,	2.58,	$Ca_2Yb_2O_5$	19- 262	
	2.91,	2.76,	3.06,	2.94,	2.56,	3.12,	4.06,	3.68,	$Ca_3(PO_4)_2$	21- 298	
•	2.91,	2.76,	2.00,	3.23,	3.11,	2.26,	2.22,	1.96,	$SrLa_2N_2O_4$	34- 311	
	2.91,	2.76,	1.52,	3.13,	2.14,	1.90,	1.69,	1.66,	YbO_2	9- 256	
	2.90,	2.76,	2.01,	3.93,	3.62,	2.18,	1.64,	1.61,	$NaCaVO_4$	14- 54	
i	2.90,	2.76,	2.00,	2.27,	3.63,	1.62,	1.83,	1.60,	Ce_2SiO_5	23-1045	
	2.90,	2.76,	1.62,	2.00,	1.70,	1.60,	1.45,	1.28,	β-TiF_3O_2	22- 490	
i	2.95,	2.75,	3.52,	3.46,	2.33,	3.86,	2.63,	4.13,	$Pb_4As_2S_7$/Sartorite	11- 76	
•	2.95,	2.75,	2.01,	2.27,	1.63,	3.75,	1.59,	1.55,	$KCaPO_4$	33-1002	
	2.95,	2.75,	2.00,	1.47,	1.29,	1.60,	2.06,	1.38,	InSb	22- 67	
	2.94,	2.75,	3.31,	1.95,	1.82,	2.00,	3.64,	3.07,	$Cd_2Cl(VO_3)_3$	19- 185	
i	2.94,	2.75,	2.67,	3.87,	3.14,	3.20,	1.84,	4.55,	$Pb_2Mg(Si_2O_7)$	22- 525	1.50
•	2.94,	2.75,	2.67,	3.14,	3.20,	4.54,	1.84,	2.81,	$Pb_2Ni(Si_2O_7)$	22- 527	1.60
	2.93,	2.75,	3.64,	2.57,	3.40,	2.88,	1.83,	1.74,	Al_2Th_3	7- 306	

FIGURE 22.4 A page from the *Search Manual* (Hanawalt Section) of the *Mineral Powder Diffraction File.* The information here is similar to that in Fig. 22.3, except that here all data entries are for minerals only. (Reproduced by permission of the International Center for Diffraction Data.)

2.94 – 2.90 (± .01)

										File No.
*	2.93$_x$	3.32$_x$	3.60$_x$	3.04$_x$	3.56$_x$	2.35$_x$	3.75$_x$	4.69$_x$	Carnallite	$KMgCl_3 \cdot 6H_2O$	24- 869
i	2.93$_x$	3.31$_x$	3.13$_x$	1.91$_x$	1.76$_x$	1.63$_x$	2.27$_x$	1.30$_x$	Wurtzite-2H, syn	n-ZnS	5- 492
	2.93$_x$	3.31$_x$	1.91$_x$	1.76$_x$	3.13$_x$	1.63$_x$	2.27$_x$	1.60$_x$	Wurtzite-2H, syn	ZnS	10- 434
i	2.91$_x$	3.30$_x$	3.44$_x$	2.75$_x$	3.76$_x$	3.02$_x$	2.28$_x$	2.07$_x$	Anderite	$AgPbSb_3S_6$	25- 596
i	2.91$_x$	3.30$_x$	2.76$_x$	3.02$_x$	1.77$_x$	2.02$_x$	1.73$_x$	4.26$_x$	Pavinsonite	$Pb_2As_2O_5$	33- 736
i	2.89$_x$	3.30$_x$	3.42$_x$	2.74$_x$	3.72$_x$	3.00$_x$	2.86$_x$	1.88$_x$	Anderite, cuprian	$Ag_2CuPb_6Sb_{12}S_{24}$	13- 462
	2.90$_x$	3.28$_x$	4.15$_x$	3.93$_x$	3.82$_x$	1.94$_x$	7.80$_x$	5.84$_x$	Chiavennite	$CaMn8e_2Si_4O_{11}(OH)_2 \cdot 2H_2O$	35- 602
e	2.89$_x$	3.28$_x$	2.79$_x$	2.59$_x$	1.91$_x$	1.53$_x$	4.46$_x$	3.57$_x$	Unnamed mineral	Ba-Ti-Si-O	17- 504
i	2.92$_x$	3.27$_x$	3.74$_x$	3.49$_x$	4.13$_x$	2.74$_x$	3.08$_x$	2.77$_x$	Meneghinite	$CuPb_{13}Sb_7S_{24}$	29- 559
*	2.92$_x$	3.27$_x$	3.03$_x$	3.96$_x$	2.07$_x$	2.03$_x$	2.62$_x$	1.94$_x$	Fabianite	$CaB_2O_4(OH)$	15- 631
	2.90$_x$	3.27$_x$	2.98$_x$	1.93$_x$	1.97$_x$	3.58$_x$	3.41$_x$	3.40$_x$	Juanite	$Ca_2(Mg,Fe)_2(Si,Al)_{12}(O,OH)_{28} \cdot 7H_2O$	29- 335
i	2.95$_x$	3.26$_x$	3.81$_x$	2.86$_x$	3.35$_x$	3.88$_x$	2.15$_x$	4.22$_x$	Semseyite	$Pb_9Sb_8S_{21}$	22-1130
e	2.94$_x$	3.26$_x$	1.70$_x$	2.50$_x$	3.63$_x$	1.63$_x$	1.36$_x$	2.19$_x$	Ilmenorutile	$Fe_2(Nb,Ta)_2Ti_{10}O_{27}$	31- 646
i	2.91$_x$	3.25$_x$	2.19$_x$	2.97$_x$	4.93$_x$	2.61$_x$	2.98$_x$	1.93$_x$	Vitoniemiite	$NaCaAl(PO_4)(F,OH)_3$	35- 598
c	2.90$_x$	3.24$_x$	3.02$_x$	3.44$_x$	2.25$_x$	3.73$_x$	2.14$_x$	3.62$_x$	Bustamite, ferroan	$(Ca,Mn)_3Si_2O_6$	33- 292
e	2.92$_x$	3.23$_x$	4.38$_x$	3.73$_x$	2.76$_x$	5.06$_x$	4.13$_x$	3.57$_x$	Seeddorite	$(Na,K)_3(Mg,Fe)_7(Al,Si)_{12}O_{30}$	23- 76
i	2.92$_x$	3.23$_x$	2.77$_x$	4.13$_x$	3.75$_x$	7.13$_x$	5.09$_x$	5.53$_x$	Osumilite	$(K,Na,Ca)(Mg,Fe)_2(Al,Fe)_3(Si,Al)_{12}O_{30} \cdot H_2O$	25- 658
	2.90$_x$	3.23$_x$	5.12$_x$	2.69$_x$	2.62$_x$	1.65$_x$	4.25$_x$	2.30$_x$	Descloizite	$(Zn,Cu)PbVO_4(OH)$	12- 537
	2.95$_x$	3.21$_x$	2.44$_x$	2.14$_x$	1.57$_x$	4.20$_x$	5.17$_x$	1.37$_x$	Ruseklevite	$(Fe,Al)_2(VO_4,PO_4)_2(OH)_3 \cdot 3H_2O$	14- 60
i	2.92$_x$	3.21$_x$	3.02$_x$	2.91$_x$	2.49$_x$	1.63$_x$	2.57$_x$	2.14$_x$	Kanoite	$(Mn,Mg)_3(Si_2O_6)$	29- 865
i	2.91$_x$	3.21$_x$	3.26$_x$	3.87$_x$	3.77$_x$	2.62$_x$	3.61$_x$	5.87$_x$	Plagionite	$Pb_5Sb_8S_{17}$	22-1129
i	2.91$_x$	3.21$_x$	3.02$_x$	2.92$_x$	2.49$_x$	1.63$_x$	2.57$_x$	2.14$_x$	Kanoite	$(Mn,Mg)_3(Si_2O_6)$	29- 865
*	2.94$_x$	3.20$_x$	3.69$_x$	2.36$_x$	2.11$_x$	3.04$_x$	1.67$_x$	2.38$_x$	Topaz	$Al_2SiO_4(F,OH)_2$	12- 765
	2.93$_x$	3.20$_x$	2.58$_x$	1.80$_x$	3.50$_x$	2.71$_x$	2.15$_x$	4.54$_x$	Carminite	$PbFe_2(AsO_4)_2(OH)_2$	12- 278
	2.91$_x$	3.20$_x$	3.00$_x$	2.63$_x$	2.19$_x$	2.10$_x$	1.68$_x$	1.57$_x$	Shcherbakovite	$NaK(Ba,K)Ti_2(Si_2O_7)_2$	31-1324
e	2.90$_x$	3.20$_x$	6.11$_x$	2.37$_x$	2.31$_x$	1.92$_x$	2.49$_x$	3.86$_x$	Unnamed mineral	K-Ca-CO_3	25- 627
	2.90$_x$	3.20$_x$	4.09$_x$	1.84$_x$	1.33$_x$	1.52$_x$	4.51$_x$	3.52$_x$	Sogdianite	$(K,Na)_3Li_2(Li,Fe,Al)_2Zr_2Si_{12}O_{30}$	21- 501
c	2.95$_x$	3.19$_x$	3.22$_x$	2.88$_x$	2.93$_x$	3.70$_x$	3.05$_x$	3.03$_x$	Baratovite	$Li_3KCa_2(Ti,Zr)_2(Si_2O_{15})F_2$	33- 811
	2.90$_x$	3.18$_x$	1.78$_x$	2.22$_x$	2.51$_x$	2.40$_x$	1.46$_x$	1.05$_x$	Leightonite	$K_2Ca_2Cu(SO_4)_4 \cdot 2H_2O$	15- 128
	2.90$_x$	3.17$_x$	2.79$_x$	2.01$_x$	1.91$_x$	1.47$_x$	2.32$_x$	2.15$_x$	Belovite	$Sr_3(Ce,Na,Ca)_2(PO_4)_3OH$	31-1350
i	2.93$_x$	3.15$_x$	3.23$_x$	4.52$_x$	2.72$_x$	2.66$_x$	2.26$_x$	2.70$_x$	Beyerite	$Ca_2PbO_2(AsO_4)_2(OH)_2$	26-1410
	2.93$_x$	3.13$_x$	1.90$_x$	1.64$_x$	1.57$_x$	2.72$_x$	1.22$_x$	1.19$_x$	Fermanite, heated	In_2TeO_6	26-1478
	2.92$_x$	3.13$_x$	2.69$_x$	4.06$_x$	1.78$_x$	5.29$_x$	2.49$_x$	4.32$_x$	Kermesite	Sb_2OS_2	11- 91
i	2.95$_x$	3.11$_x$	2.93$_x$	1.78$_x$	4.35$_x$	1.98$_x$	2.68$_x$	2.14$_x$	Okenoganite	$(Na,Ca)_3Ln_{12}Si_{24}O_{72}F_{12}$	35- 483
c	2.94$_x$	3.11$_x$	3.22$_x$	2.84$_x$	3.67$_x$	3.41$_x$	2.58$_x$	2.89$_x$	Triploidite	$Mn_2{}^{+}Fe_2{}^{3+}(PO_4)_4(OH)$	26-1239
i	2.93$_x$	3.11$_x$	3.04$_x$	2.66$_x$	8.84$_x$	2.69$_x$	4.51$_x$	3.58$_x$	Kulanite	$Ba(Fe,Mn,Mg)_2Al_2(PO_4)_3(OH)_3$	29- 170
	2.94$_x$	3.10$_x$	3.19$_x$	1.80$_x$	3.41$_x$	2.58$_x$	2.31$_x$	2.15$_x$	Triploidite	$(Mn,Fe)_2PO_4(OH)$	26-1240
	2.94$_x$	3.10$_x$	3.00$_x$	2.16$_x$	3.44$_x$	1.65$_x$	1.43$_x$	1.07$_x$	Manganberzeliingtonite	$Ca_2(Mn,Fe)Fe_2Si_3O_{12}OH$	26- 313
	2.93$_x$	3.09$_x$	3.18$_x$	1.79$_x$	3.37$_x$	2.57$_x$	2.29$_x$	2.14$_x$	Wolfeite	$(Fe,Mn)_2(PO_4)(OH)$	5- 612
i	2.92$_x$	3.09$_x$	2.65$_x$	8.81$_x$	3.03$_x$	2.68$_x$	4.49$_x$	2.69$_x$	Penikisite	$Ba(Mg,Fe)_3Al_2(PO_4)_3(OH)_3$	29- 169
	2.94$_x$	3.08$_x$	2.79$_x$	3.44$_x$	3.26$_x$	2.24$_x$	2.08$_x$	1.88$_x$	Kalborsite	$K_6BAl_3Si_9O_{30}(OH)_2Cl$	33- 999
	2.91$_x$	3.08$_x$	1.64$_x$	4.69$_x$	4.81$_x$	2.36$_x$	4.20$_x$	4.27$_x$	Canasite	$(Na,K)_6Ca_9Si_{12}O_{30}(OH,F)_4$	13- 553
i	2.90$_x$	3.08$_x$	1.76$_x$	3.06$_x$	3.31$_x$	3.27$_x$	2.16$_x$	2.73$_x$	Pectolite	$NaCa_2HSi_3O_9$	33-1223
e	2.92$_x$	3.07$_x$	2.59$_x$	1.84$_x$	1.50$_x$	3.68$_x$	1.90$_x$	11.0$_x$	Samarskite, heated	$(Y,U,Fe)(Nb,Ta,Ti)_2O_6$	4- 617
i	2.94$_x$	3.06$_x$	1.89$_x$	3.96$_x$	2.63$_x$	2.48$_x$	1.82$_x$	2.20$_x$	Rosenbuschite	$(Na,Ca)_3(Fe,Ti,Zr)(SiO_3)_3F$	14- 447
	2.92$_x$	3.06$_x$	4.21$_x$	3.52$_x$	3.24$_x$	6.15$_x$	6.51$_x$	2.18$_x$	Kasolite	$Pb(UO_2)SiO_4 \cdot H_2O$	29- 788
e	2.92$_x$	3.04$_x$	2.99$_x$	3.32$_x$	2.08$_x$	1.56$_x$	1.52$_x$	1.97$_x$	Mimetite, phosphatian	$Pb_5Cl((As,P)O_4)_3$	13- 124
i	2.92$_x$	3.04$_x$	3.35$_x$	2.78$_x$	2.91$_x$	3.83$_x$	1.91$_x$	2.56$_x$	Reinhardbraunsite	$Ca_5(SiO_4)_2(OH)_2$	29- 380
i	2.89$_x$	3.03$_x$	3.19$_x$	2.52$_x$	1.91$_x$	1.75$_x$	2.75$_x$	2.63$_x$	Rustumite	$Ca_{10}(Si_2O_7)_2SiO_4Cl_2(OH)_2$	18- 305
e	2.95$_x$	3.02$_x$	3.09$_x$	5.50$_x$	2.97$_x$	2.66$_x$	4.43$_x$	2.80$_x$	Yttropyrochlore	$(Y,Ce,Nd,Th)(Nb,Ti,Ta)_2O_6$	18- 765
i	2.91$_x$	3.02$_x$	2.90$_x$	3.21$_x$	2.58$_x$	1.63$_x$	1.49$_x$	1.39$_x$	Pigeonite	$(Fe,Mg,Ca)SiO_3$	13- 421
i	2.90$_x$	3.02$_x$	3.21$_x$	2.91$_x$	2.58$_x$	1.63$_x$	1.49$_x$	1.39$_x$	Pigeonite	$(Fe,Mg,Ca)SiO_3$	13- 421
	2.94$_x$	3.01$_x$	2.81$_x$	1.73$_x$	2.25$_x$	1.98$_x$	1.66$_x$	1.63$_x$	Sahlinite	$Pb_{14}(AsO_4)_2O_9Cl_4$	22- 664
	2.89$_x$	3.01$_x$	5.75$_x$	3.20$_x$	3.93$_x$	3.08$_x$	2.82$_x$	5.01$_x$	Realgar, high, syn	β-AsS	25- 57
i	2.95$_x$	3.00$_x$	4.84$_x$	3.78$_x$	3.70$_x$	2.50$_x$	2.88$_x$	1.73$_x$	Huebnerite, syn	MnWO$_4$	13- 434
	2.94$_x$	3.00$_x$	3.06$_x$	3.20$_x$	2.88$_x$	2.53$_x$	2.20$_x$	2.11$_x$	Roeblingite	$Ca_2Pb_3(SO_4)_2Si_2O_{14}(OH)_{10}$	18- 292
	2.94$_x$	3.00$_x$	1.58$_x$	2.65$_x$	1.70$_x$	1.86$_x$	3.71$_x$	2.21$_x$	Tantalaeschynite-(Y), heated	$(Y,Ce,Ca)(Ta,Ti,Nb)_2O_6$	26- 1
*	2.90$_x$	3.00$_x$	2.89$_x$	4.18$_x$	2.42$_x$	2.09$_x$	2.08$_x$	4.16$_x$	Arcanite, syn	K_2SO_4	5- 613
i	2.91$_x$	2.99$_x$	3.07$_x$	1.57$_x$	1.51$_x$	2.59$_x$	1.85$_x$	2.77$_x$	Aeschynite-(Y), syn	YTiNbO$_6$	20-1401
i	2.89$_x$	2.99$_x$	2.29$_x$	1.93$_x$	4.96$_x$	1.50$_x$	5.77$_x$	1.90$_x$	Alunite	$(K,Na)Al_3(SO_4)_2(OH)_6$	14- 136
e	2.91$_x$	2.98$_x$	2.52$_x$	2.49$_x$	2.20$_x$	2.02$_x$	1.41$_x$	2.54$_x$	Diopside, manganoan	$(Ca,Mn)(Mg,Fe,Mn)Si_2O_6$	22- 534
i	2.95$_x$	2.97$_x$	4.78$_x$	3.76$_x$	3.67$_x$	2.49$_x$	2.86$_x$	2.39$_x$	Wolframite, syn	FeMn(WO$_4$)$_2$	12- 727
i	2.94$_x$	2.97$_x$	3.11$_x$	2.93$_x$	1.78$_x$	4.35$_x$	1.98$_x$	2.68$_x$	Okenoganite	$(Na,Ca)_3Ln_{12}Si_{24}O_{72}F_{12}$	35- 483
	2.93$_x$	2.97$_x$	1.83$_x$	11.7$_x$	6.00$_x$	3.13$_x$	4.21$_x$	4.00$_x$	Fedorite	$(K,Na)_3(Ca,Na)_{13}Si_{26}O_{66}(OH,F)_7 \cdot H_2O$	19- 466
	2.89$_x$	2.94$_x$	4.43$_x$	3.29$_x$	2.61$_x$	1.39$_x$	1.87$_x$	3.05$_x$	Joaquinite	$Ba_2NaCe_2FeTi_2Si_8O_{26}(OH)$	26-1034
*	2.91$_x$	2.93$_x$	3.73$_x$	4.69$_x$	3.62$_x$	2.47$_x$	2.46$_x$	2.86$_x$	Sanmartinite, syn	ZnWO$_4$	15- 774
*	2.90$_x$	2.92$_x$	4.37$_x$	3.79$_x$	2.73$_x$	2.51$_x$	4.66$_x$	2.45$_x$	Pumpellyite	$Ca_2MgAl_2(Si_2O_{11})(OH)_2 \cdot H_2O$	25- 156
*	2.93$_x$	2.91$_x$	3.73$_x$	4.69$_x$	3.62$_x$	2.47$_x$	2.46$_x$	2.86$_x$	Sanmartinite, syn	ZnWO$_4$	15- 774
c	2.89$_x$	2.91$_x$	3.24$_x$	3.02$_x$	3.44$_x$	2.25$_x$	3.73$_x$	2.14$_x$	Bustamite, ferroan	$(Ca,Mn)_3Si_2O_6$	33- 292
c	2.91$_x$	2.89$_x$	3.24$_x$	3.02$_x$	3.44$_x$	2.25$_x$	3.73$_x$	2.14$_x$	Bustamite, ferroan	$(Ca,Mn)_3Si_2O_6$	33- 292
i	2.95$_x$	2.88$_x$	2.78$_x$	3.02$_x$	2.84$_x$	2.71$_x$	4.54$_x$	3.30$_x$	Ilmenite	$Y_4(SiO_4)(CO_3)$	35- 640
i	2.89$_x$	2.87$_x$	5.90$_x$	6.60$_x$	4.41$_x$	4.72$_x$	4.37$_x$	2.94$_x$	Mesolite	$Na_2Ca_2Al_6Si_9O_{30} \cdot 9H_2O$	24-1064
	2.95$_x$	2.86$_x$	1.76$_x$	1.14$_x$	3.31$_x$	2.77$_x$	2.42$_x$	1.55$_x$	Nordite-(La)	$Na_2(nSrMnSi_2O_7)_n$	27- 672
e	2.93$_x$	2.86$_x$	2.14$_x$	1.85$_x$	2.06$_x$	2.80$_x$	3.23$_x$	1.99$_x$	Tyrrellite-1Tc	$Co_2B_2O_5(OH)_2$	26- 2
	2.91$_x$	2.86$_x$	2.61$_x$	1.72$_x$	1.19$_x$	2.64$_x$	1.86$_x$	1.14$_x$	Vysotskite	(Pd,Ni)S	15- 151
	2.90$_x$	2.86$_x$	2.74$_x$	3.71$_x$	3.51$_x$	3.24$_x$	2.84$_x$	5.56$_x$	Kentrolite, ferroan	$Pb_2(Mn,Fe)_2Si_2O_9$	20- 586
c	2.95$_x$	2.84$_x$	2.86$_x$	3.08$_x$	2.54$_x$	2.90$_x$	3.82$_x$	3.29$_x$	Latiumite	$(Ca,K)_4(Si,Al)_2O_4(SO_4,CO_3)$	25-1202
	2.91$_x$	2.84$_x$	2.82$_x$	1.87$_x$	3.99$_x$	2.67$_x$	3.43$_x$	3.21$_x$	Svabite	$Ca_5(AsO_4)_3(OH,Cl,F)$	19- 215
	2.94$_x$	2.82$_x$	3.10$_x$	4.25$_x$	4.05$_x$	3.35$_x$	3.19$_x$	2.58$_x$	Eudialyte, yttrian	$Na_{12}(Ca,Ln)_3Zr_3Si_{25}O_{73}(OH)_3$	25- 814
c	2.93$_x$	2.82$_x$	2.51$_x$	1.80$_x$	1.75$_x$	1.81$_x$	1.52$_x$	1.54$_x$	Zirkelite	$CaZrTi_2O_7$	34- 167
*	2.92$_x$	2.82$_x$	2.03$_x$	1.93$_x$	1.47$_x$	3.20$_x$	1.83$_x$	1.97$_x$	Strontium-apatite, syn	$Sr_5(PO_4)_3OH$	33-1348
	2.90$_x$	2.82$_x$	2.80$_x$	3.98$_x$	3.47$_x$	2.68$_x$	1.88$_x$	2.03$_x$	Johnbaumite	$Ca_5(AsO_4)_3(OH)$	33- 265
	2.89$_x$	2.82$_x$	2.78$_x$	2.14$_x$	2.05$_x$	1.99$_x$	1.84$_x$	1.83$_x$	Hilgardite-1Tc, strontian	$(Ca,Sr)_2B_5O_9(OH)_5Cl$	11- 405
	2.93$_x$	2.81$_x$	8.43$_x$	2.23$_x$	6.18$_x$	4.22$_x$	2.10$_x$	3.32$_x$	Kotoite	$Mg_3B_2O_6$	14- 393
	2.89$_x$	2.81$_x$	3.22$_x$	6.79$_x$	3.99$_x$	2.41$_x$	2.01$_x$	1.79$_x$	Kotoite	$Mg_3B_2O_6$	14- 393
*	2.92$_x$	2.79$_x$	4.21$_x$	6.12$_x$	4.36$_x$	3.44$_x$	3.19$_x$	2.45$_x$	Kotoite	$Mg_3B_2O_6$	14- 393
*	2.92$_x$	2.79$_x$	2.02$_x$	2.06$_x$	1.48$_x$	1.44$_x$	1.21$_x$	1.66$_x$	Spodumene	n-LiAlSi$_2$O$_6$	33- 786
i	2.89$_x$	2.79$_x$	2.59$_x$	2.68$_x$	2.67$_x$	2.40$_x$	2.29$_x$	2.10$_x$	Tin, syn	Sn	4- 673
i	2.89$_x$	2.78$_x$	2.66$_x$	2.17$_x$	2.32$_x$	1.87$_x$	2.54$_x$	1.67$_x$	Clinozoisite	$Ca_2(Al,Fe)Al_2(SiO_4)_3OH$	21- 138
i	2.95$_x$	2.75$_x$	3.52$_x$	3.46$_x$	2.33$_x$	3.86$_x$	2.63$_x$	4.13$_x$	Berentsite	$Na_2AlH_3(CO_3)_4F_2$	35- 693
									Sartorite	PbAs$_2$S$_4$	11- 76

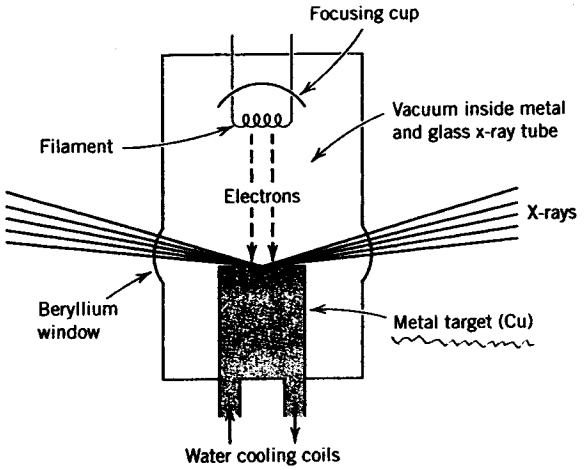

FIG. 7.32. Schematic representation of a sealed vacuum X-ray tube. The tungsten filament is heated to very high temperature, making electrons boil off. The differential voltage between the filament and the target metal accelerates the electrons toward the target. When the electrons strike the target, X-rays are produced that are able to leave the X-ray tube housing through beryllium windows.

$\lambda_{Cu} = 1.5418$ Å

X-Ray Powder Diffraction and Mineral Identification

The relative rarity of well-formed crystals and the difficulty of achieving the precise orientation required by single-crystal methods led to the discovery of the *powder method* of X-ray investigation. In X-ray diffraction studies of powders, the original specimen is ground as finely as possible and bonded with an amorphous material into a small spindle (for powder film methods) or mounted on a glass slide, or in a special rectangular sample holder (for powder diffractometer techniques). The *powder mount* consists ideally of crystalline particles in completely random orientation. To ensure randomness of orientation of these tiny particles with respect to the impinging X-ray beam, the spindle mount (used in film cameras) is generally rotated in the path of the beam during exposure.

When a beam of monochromatic X-ray strikes the mount, all possible diffractions take place simultaneously. If the orientation of the crystalline particles in the mount is truly random, for each family of atomic planes with its characteristic interplanar spacing (d), there are many particles whose orientation is such that they make the proper θ angle with the incident beam to satisfy the *Bragg law*: $n\lambda = 2d \sin \theta$. The diffraction maxima from a given set of planes form cones with the incident beam as axis and the internal angle 4θ. Any set of atomic planes yields a series of nested cones corresponding to "reflections" of the first, second, third, and higher orders ($n = 1, 2, 3, \ldots$). Different families of planes with different interplanar spacings will satisfy the Bragg law at appropriate values of θ for different integral values of n, thus giving rise to separate sets of nested cones of "reflected" rays.

If the rays forming these cones are permitted to fall on a flat photographic plate at right angles to the incident beam, a series of concentric circles will result (Fig. 7.43). However, only "reflections" with small values of the angle 2θ can be recorded in this manner.

In order to record all the possible diffraction cones that may occur in three dimensions (see Figs. 7.36 and 7.37) a film method is used in which the film is wrapped around the inside of a cylindrical camera. This camera is known as a *powder camera* in which the film fits snugly to the inner curve of the camera (see Fig. 7.44*a*). This type of mounting is known as the *Straumanis method.* Figure 7.44*b* shows the circular film strip with two holes cut into it, one to allow the X-ray beam to enter the camera and the other for a lead-lined beam catcher. Although this powder camera method has been used extensively for mineral identification, the X-ray *powder diffractometer* is the instrumental method currently used most often. This powerful analytical tool uses essentially monochromatic X-radiation and a finely powdered sample, as does the powder film method, but records the information about the "reflections" present as a graphical recording, or as electronic counts (X-ray counts) that can be stored and printed out by computer.

The sample for powder diffractometer analysis is prepared by grinding it to a fine powder, which is then spread uniformly over the surface of a glass slide, using a small amount of adhesive binder. (If enough powder is available it can be compressed

FIG. 7.43. X-ray diffraction from a powder mount recorded on a flat plate.

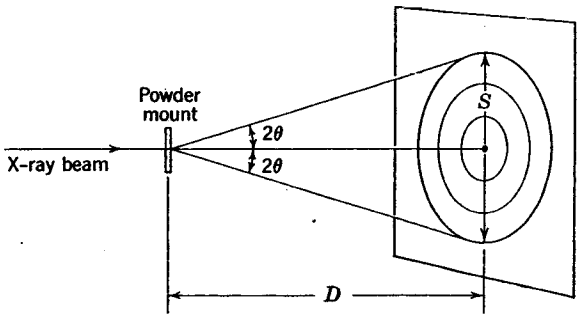

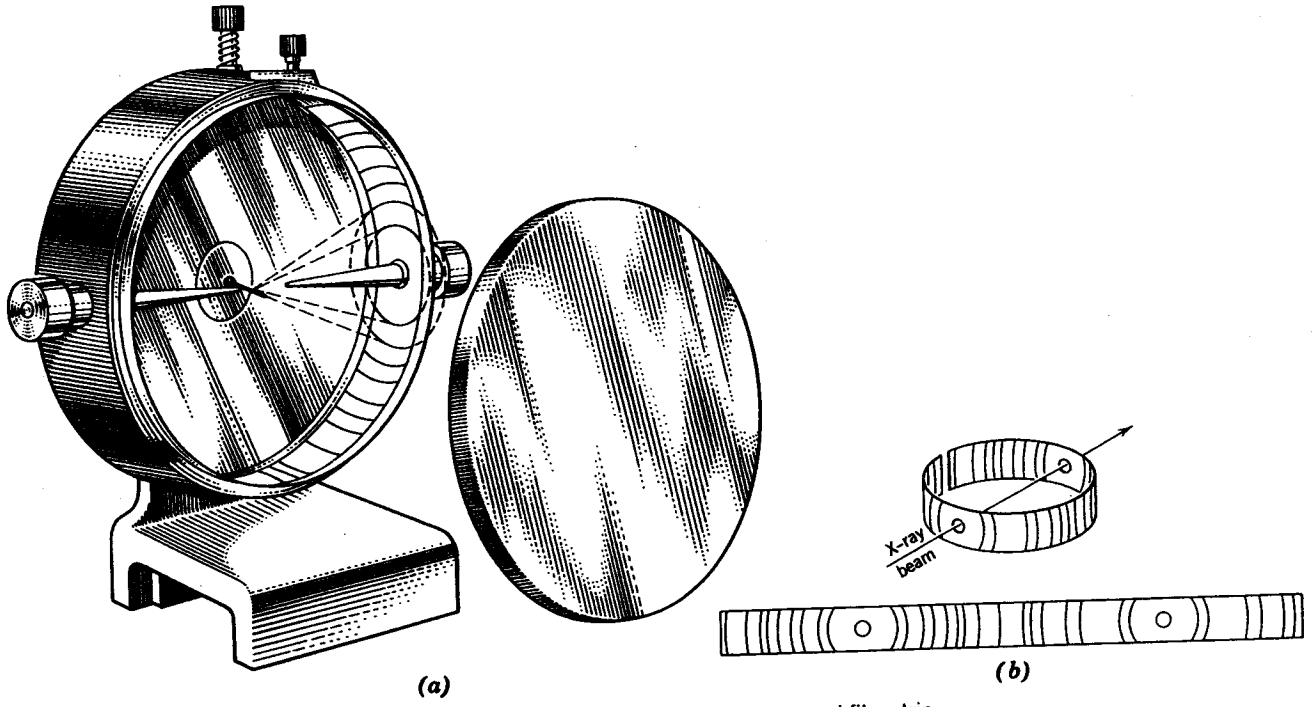

FIG. 7.44. *(a)* Metal powder diffraction camera with a powder spindle in the center and film strip against the inner cylindrical wall of the camera. *(b)* Circular film strip with curved lines that represent the conical "reflections" produced inside the camera.

into a rectangular sample holder.) The instrument is so constructed that the sample, when clamped in place, rotates in the path of a collimated X-ray beam while an X-ray detector, mounted on an arm, rotates about it to pick up the diffracted X-ray signals (see Fig. 7.45). When the instrument is set at zero position, the X-ray beam is parallel to the base of the sample holder and passes directly into the X-ray detector. The slide mount and the counter are driven by a motor through separate gear trains so that, while the sample rotates through the angle θ, the detector rotates through 2θ.

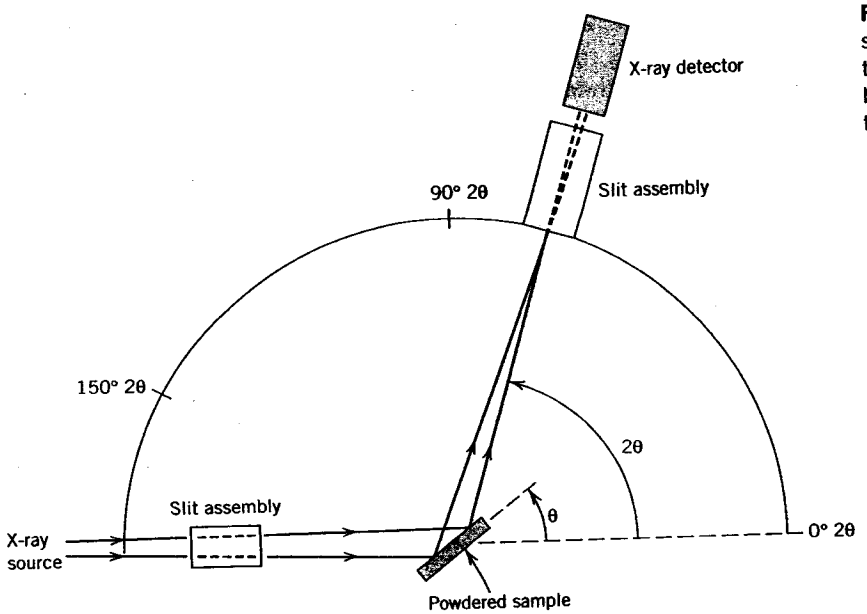

FIG. 7.45. Schematic illustration of the essential components of a powder X-ray diffractometer. In such an instrument the sample holder rotates (θ)° while the detector arm rotates 2(θ)°.

If the specimen has been properly prepared, there will be thousands of tiny crystalline particles in random orientation. As in powder photography, all possible "reflections" from atomic planes take place simultaneously. Instead of recording all of them on a film at one time, however, the X-ray detector maintains the appropriate geometrical relationship to receive each diffraction maximum separately.

In operation, the sample, the X-ray detector, and the recording device are activated simultaneously. If an atomic plane has an interplanar spacing (d) such that a reflection occurs at $\theta = 20°$, there is no evidence of this reflection until the counting tube has been rotated through 2θ, or 40°. At this point the diffracted beam enters the X-ray detector, causing it to respond. The pulse thus generated is amplified and causes an electronic response on a vertical scale that represents peak height. The angle 2θ at which the diffraction occurs is read on a horizontal scale. The heights of the peaks are directly proportional to the intensities of the diffraction effects. An example of a diffractometer tracing for low quartz is given in Figure 7.46. The 2θ positions of the diffraction peaks in such a tracing can be read off directly or they can be tabulated as 2θ positions by an online computer. The interplanar spacings giving rise to them are calculated using the equation $n\lambda = 2d \sin \theta$.

Once a diffractometer tracing has been obtained and the various diffraction peaks have been tabulated in a sequence of decreasing interplanar spacings (d), together with their relative intensities (I, with the strongest peak represented by 100 and all the other peaks scaled with respect to 100), the investigator is ready to begin the mineral identification process. Through a computer search technique (doing searches for comparable or identical diffraction patterns on the basis of the strongest lines or the largest interplanar spacings), the diffraction pattern of an unknown can be compared with records stored in the Powder Diffraction File (PDF) published by the International Center for Diffraction Data (ICDD). This file is primarily available on CD-ROM and is compatible with PC, VAX/VMS, and Macintosh platforms.

The Powder Diffraction File is the world's largest and most complete collection of X-ray powder diffraction patterns. The PDF contains more than 70,000 experimental patterns compiled by the ICDD since 1941, as well as more than 42,000 calculated patterns. Each pattern includes a table of interplanar (d) spacings, relative intensities (I), and Miller indices, as well as additional information such as chemical formula, compound name, mineral name, structural formula, crystal system, physical data, experimental parameters, and references. An example printout for low quartz from this file is shown in Fig. 7.47. Entries are indexed to allow for subfile searches of inorganics, organics, minerals, metals and alloys, common phases, pharmaceuticals, zeolites, and many others.

By this outlined comparative search procedure a completely unknown substance may generally be identified in a short time using a very small volume of sample.

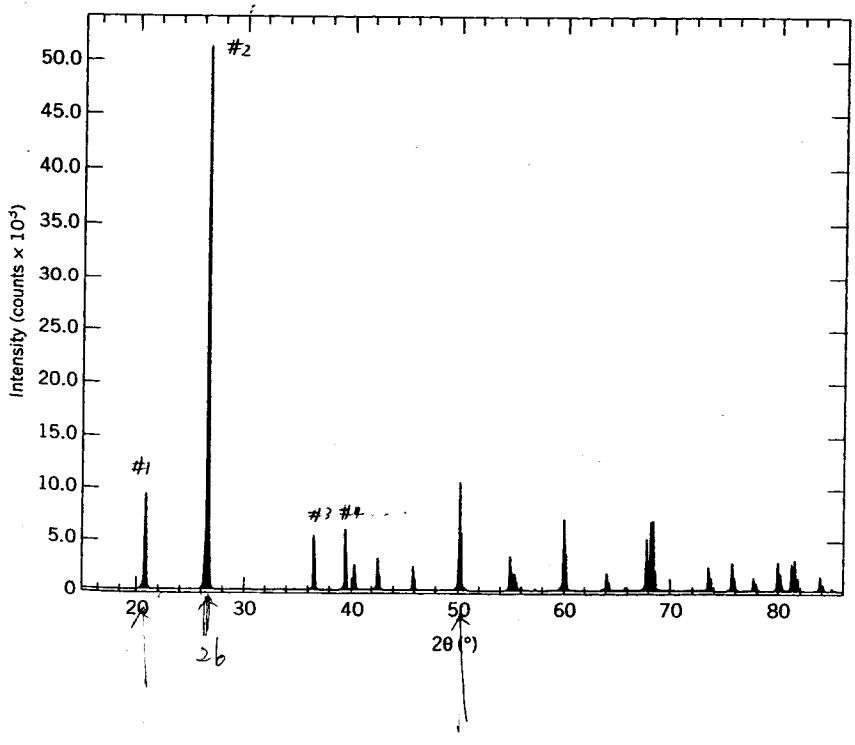

FIG. 7.46. X-ray powder diffractometer tracing for a finely powdered sample of low quartz.

PDF Card

PDF#33-1161 (Deleted Card): QM = Star (+); d = Diffractometer, I = Diffractometer

Quartz, syn
SiO2

Radiation = CuKa1
Calibration = Internal (Si)
Ref = Natl. Bur. Stand. (U.S.) Monogr. 25, 18 61 (1981)
Lambda = 1.540598
d-Cutoff =
Filter =
I/Ic (RIR) = 3.6

Hexagonal—(Unknown), P3221(154)
Cell = 4.9134 × 5.4053
Density (c) = 2.649 Density (m) = 2.656 Mwt = 60.08 Vol = 113.01
Ref = Ibid.
Z = 3 mp =
Pearson = hP9 (O2 Si)
F(30) = 76.8 (.0126,31)

NOTE: Sample from the Glass Section at NBS, Gaithersburg, MD, USA, ground single-crystals of optical quality. To replace 5-490 and validated by calculated pattern. Plus 6 additional reflections to 0.9089. Pattern taken at 25 C. Pattern reviewed by Holzer, J., McCarthy, G., North Dakota State Univ., Fargo, ND, USA, ICDD Grant-in-Aid (1990). Agrees well with experimental and calculated patterns. Deleted by 46-1045, higher F#N, more complete, LRB 1/95.

Color: Colorless

Strong Line: 3.34/X 4.26/2 1.82/1 1.54/1 2.46/1 2.28/1 1.37/1 1.38/1 2.13/1 2.24/1

39 Lines, Wavelength to Compute Theta = 1.54056A (Cu), 1%-Type = (Unknown)

#	d(A)	I(f)	h	k	l	2-Theta	Theta	1/(2d)	#	d(A)	I(f)	h	k	l	2-Theta	Theta	1/(2d)
1	4.2570	22.0	1	0	0	20.850	10.425	0.1175	21	1.2285	1.0	2	2	0	77.660	38.830	0.4070
2	3.3420	100.0	1	0	1	26.651	13.326	0.1495	22	1.1999	2.0	2	1	3	79.875	39.938	0.4167
3	2.4570	8.0	1	1	0	36.541	18.271	0.2035	23	1.1978	1.0	2	2	1	80.044	40.022	0.4174
4	2.2820	8.0	1	0	2	39.455	19.727	0.2191	24	1.1843	3.0	1	1	4	81.145	40.572	0.4222
5	2.2370	4.0	1	1	1	40.283	20.141	0.2235	25	1.1804	3.0	3	1	0	81.470	40.735	0.4236
6	2.1270	6.0	2	0	0	42.464	21.232	0.2351	26	1.1532	1.0	3	1	1	83.818	41.909	0.4336
7	1.9792	4.0	2	0	1	45.808	22.904	0.2526	27	1.1405	1.0	2	0	4	84.969	42.484	0.4384
8	1.8179	14.0	1	1	2	50.139	25.070	0.2750	28	1.1143	1.0	3	0	3	87.461	43.731	0.4487
9	1.8021	1.0	0	0	3	50.610	25.305	0.2775	29	1.0813	2.0	3	1	2	90.855	45.428	0.4624
10	1.6719	4.0	2	0	2	54.867	27.434	0.2991	30	1.0635	1.0	4	0	0	92.819	46.410	0.4701
11	1.6591	2.0	1	0	3	55.327	27.663	0.3014	31	1.0476	1.0	1	0	5	94.662	47.331	0.4773
12	1.6082	1.0	2	1	0	57.236	28.618	0.3109	32	1.0438	1.0	4	0	1	95.115	47.558	0.4790
13	1.5418	9.0	2	1	1	59.947	29.973	0.3243	33	1.0347	1.0	2	1	4	96.223	48.112	0.4832
14	1.4536	1.0	1	1	3	63.999	32.000	0.3440	34	1.0150	1.0	2	2	3	98.734	49.367	0.4926
15	1.4189	1.0	3	0	0	65.759	32.879	0.3524	35	0.9898	1.0	4	0	2	102.195	51.098	0.5052
16	1.3820	6.0	2	1	2	67.748	33.874	0.3618	36	0.9873	1.0	3	1	3	102.556	51.278	0.5064
17	1.3752	7.0	2	0	3	68.128	34.064	0.3636	37	0.9783	1.0	3	0	4	103.880	51.940	0.5111
18	1.3718	8.0	3	0	1	68.321	34.160	0.3645	38	0.9762	1.0	3	2	0	104.195	52.098	0.5122
19	1.2880	2.0	1	0	4	73.460	36.730	0.3882	39	0.9636	1.0	2	0	5	106.141	53.071	0.5189
20	1.2558	2.0	3	0	2	75.668	37.834	0.3982									

FIG. 7.47. Example of the printout for SiO_2, low quartz, as obtained from the powder diffraction file (PDF-2) licensed by the International Center for Diffraction Data (JCPDS), 12 Campus Boulevard, Newton Square, PA., 19073-3273; copyright © JCDPS-ICDD, 1999. The printout was obtained using Jade 5.0 from Materials Data Inc. (MDI).

The powder method is of wider usefulness, however, and there are several other applications in which it is of great value. Variations in chemical composition of a known substance involve the substitution of ions, generally of a somewhat different size, in specific sites in a crystal structure. As a result of this substitution the unit cell dimensions and hence the interplanar spacings are slightly changed, and the positions of the lines in the powder diffractogram corresponding to these interplanar spacings are shifted accordingly. By measuring these small shifts in position of the lines in powder patterns of substances of known structure, changes in chemical composition may often be accurately detected. Figure 7.48 illustrates a variation diagram that correlates unit cell dimensions (b and unit cell volume, V) and changes in the position of a specific diffraction maximum (1, 11, 0) with composition in the cummingtonite-grunerite series.

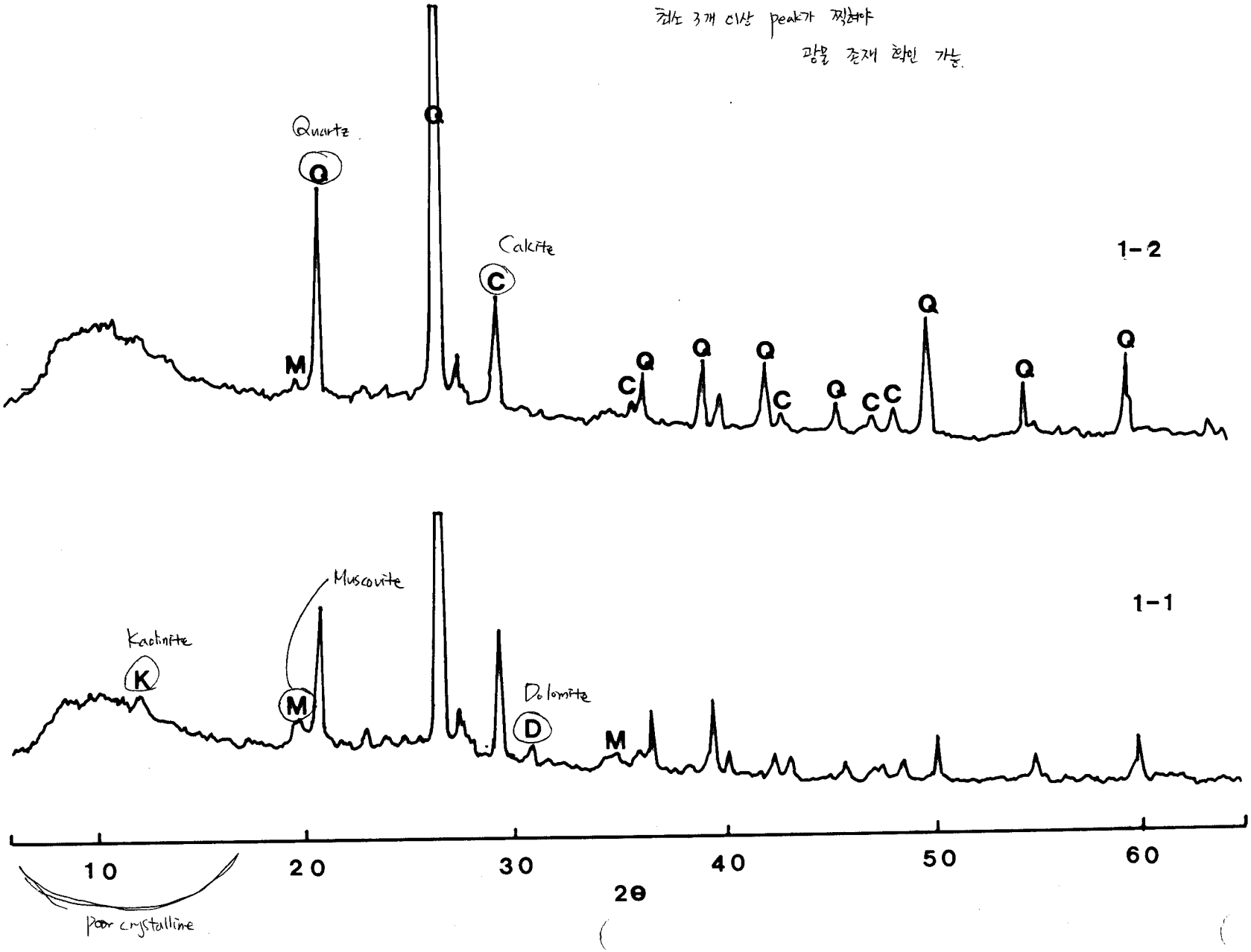
최소 3개 이상 peak가 찍혀야
광물 존재 확인 가능
Quartz
Q
Calcite
C
M
1-2
1-1
Kaolinite
K
Muscovite
Dolomite
D
10
20
30
40
50
60
2θ
Poor crystalline